Hindawi
Journal of Nanomaterials
Volume 2019, Article ID 4825432, 10 pages
https://doi.org/10.1155/2019/4825432

Research Article

One-Pot Synthesis of Titanate Nanotubes Decorated with Anatase Nanoparticles Using a Microwave-Assisted Hydrothermal Reaction

Suziete B. S. Gusmão,[1] Anupama Ghosh,[2] Thalles M. F. Marques,[3] Odair P. Ferreira,[4] Anderson O. Lobo,[1,5] Josy A. O. Osajima,[1] Cleanio Luz-Lima,[2] Romulo R. M. Sousa,[1] Jose M. E. Matos,[6] and Bartolomeu C. Viana[1,2]

[1]*Interdisciplinary Laboratory of Advanced Materials, Materials Science and Engineering Graduate Program, Federal University of Piaui, Teresina, PI CEP 64049-550, Brazil*
[2]*FisMat, Department of Physics, Federal University of Piaui, Teresina, PI CEP 64049-550, Brazil*
[3]*Federal Institute of Technology, Ciência e Tecnologia do Piauí, São João do Piauí, PI 64760-000, Brazil*
[4]*Laboratory of Advanced Functional Materials, Department of Physics, Federal University of Ceará, Fortaleza, CE CEP 60455-900, Brazil*
[5]*Department of Chemistry, Massachusetts Institute of Technology, Cambridge, MA 02139, USA*
[6]*Department of Chemistry, Federal University of Piaui, Teresina, PI CEP 64049-550, Brazil*

Correspondence should be addressed to Anupama Ghosh; anupama1984@gmail.com
and Bartolomeu C. Viana; bartolomeu@ufpi.edu.br

Received 27 November 2018; Accepted 20 January 2019; Published 14 March 2019

Guest Editor: Zhen Yu

A nanoheterostructure of titanate nanotubes decorated with anatase nanoparticles (TiNT@AnNP) was synthesized for the first time by a microwave-assisted hydrothermal one-pot reaction. Characterization by X-ray diffraction, Raman spectroscopy, scanning electron microscopy, energy-dispersive X-ray spectroscopy, high-resolution transmission electron microscopy, selected-area electron diffraction, and X-ray photoelectron spectroscopy showed highly crystalline and nanometer-sized TiNT@AnNP. The synthesized TiNT@AnNP degraded an anionic dye (Remazol blue) more efficiently under UV-visible light (380–780 nm) than a commercial anatase-TiO_2 precursor. We correlated this increased efficiency of photodegradation to the large surface area and the efficient separation of photoinduced electron-hole pairs. Finally, we propose a mechanism to highlight the influence of a microwave-assisted hydrothermal synthesis in the production of TiNT@AnNP for environmental applications.

1. Introduction

Nanostructured titanium oxide- (TiO_2-) based compounds are one of the most intensely studied families of inorganic oxides in the literature [1]. Their fascinating structural, electronic, and biological properties make them useful for various environmental, energy, and biomedical applications, such as adsorption, photochemical degradation, Li-ion batteries, photovoltaic cells, oil-water separation, and antibacterial activity [1]. A layered titanate nanostructure has strong structural similarity to the anatase phase of TiO_2, with similar building blocks of TiO_6 octahedrons, connected by corner- and edge-sharing oxygen atoms forming negatively charged two-dimensional sheets, which facilitates fast ion diffusion, leading to exchange and intercalation, and the increased surface area facilitates photocatalytic application [2]. Different synthetic techniques, such as template-based methods, sol-gel process, anodic oxidation, and hydrothermal treatment have been used to generate titanate nanostructures with different morphologies and properties [3]. A vast

number of structure-property relationship studies led scientists not only to apply these materials in various fields but also to understand the basic mechanism of the phase transformation between crystalline phases of titania and titanates, as well as to the possibility to generate new functional materials with tailored properties [4]. Formation of a TiO_2- (anatase-) trititanate heterostructure is one example, which has been a hot topic recently because of its increased efficiency in photocatalysis and photodegradation [5]. These properties have been associated with different structural and electronic properties, such as the band gap and the surface area [5, 6]. TiO_2- (anatase-) trititanate heterostructures are easily interconverted by low-energy-requiring pathways as predicted by calculations because of the structural similarity between trititanate and TiO_2 (anatase) [7]. These behaviors are associated with either a topochemical reaction involving dehydration of the titanate layers, followed by an in situ rearrangement of the structural units leading to titanate-to-anatase phase transformation [8], or a gradual decomposition and dissolution of the titanate surface, causing the production of $Ti(OH)_4$ fragments, which undergo dehydration resulting in Ti–O–Ti bridge formation, thereby starting the nucleation of the anatase phase [9]. Synthesis of a titanate-anatase heterostructure was achieved by controlled thermal annealing, causing a two-step dehydration, the first step being at the layers, leading to a decrease in interlayer distance, and the second step resulting in partial destruction of the tube, forming anatase particles on titanate nanotubes at 350–400°C [10]. Milder postsynthetic treatment of titanate nanotubes (48 h stirring in 0.05 M HNO_3 at 70°C) generated titanate nanotubes decorated with anatase nanocrystals of 5–20 nm in diameter [11, 12]. Postsynthetic hydrothermal treatment of titanate tubes at 150°C for 24 h yielded phase transformation of trititanate to anatase, which exhibited an increased surface area as well as a decreased band gap, which is ideal for photocatalysis reactions [13].

In recent years, another great advance in the synthetic strategy has been achieved by using microwave heating in place of conventional heating as it is a faster and more efficient heating method [14]. The first microwave adaptation of the Kasuga-introduced conventional alkaline hydrothermal synthesis of titanate nanotubes from anatase TiO_2 [15] was in 2005 by Wang et al. [16]; the reaction time was reduced to 6 h. Recently, detailed analysis was performed on microwave synthesis of titanate nanostructures to understand and evaluate the advantage of microwave irradiation compared to conventional heat treatment, and it was found that it not only decreases the reaction time manyfold but also helps to obtain nanostructures with a greater surface area compared to the conventional method, which, in turn, can help the nanostructures act as a better catalyst [17, 18]. The careful selection of the reaction time and temperature can lead to a trititanate-anatase mixed phase final product because of incomplete conversion to titanate nanotubes and partial retention of the starting structure (anatase), which can give rise to better photoactivity than either a pure anatase phase or a pure trititanate phase [19, 20]. Additionally, a microwave-assisted hydrothermal synthesis can give rise to the formation of anatase nanostructures under conditions similar to those that result in titanate nanotubes in conventional hydrothermal synthesis, possibly due to the rapid molecular rearrangement caused by uniform microwave irradiation [21].

Herein, a very simple one-pot synthesis of a titanate-anatase nanostructure has been realized for the first time using a microwave-assisted alkaline hydrothermal method starting from pure anatase powder. Long, thin titanate nanotubes decorated with anatase nanocrystals of average diameter 3.3 nm (TiNT@AnNP) were obtained. This unique nanoheterostructure was thoroughly characterized by high-resolution transmission electron microscopy (HRTEM) and was found to contain anatase and titanate nanostructures, corroborating the findings of X-ray diffraction (XRD), Raman spectroscopy, and selected-area electron diffraction (SAED) analysis. The synthesized TiNT@AnNP photocatalytically degraded the dye Remazol blue more efficiently than a commercial anatase-TiO_2 precursor did. We propose and discuss a mechanism to explain the influence of the microwave-assisted hydrothermal route to produce TiNT@AnNP. Our method is an alternative and economic one-pot synthetic route to achieve a better catalyst.

2. Experimental Part

2.1. Synthesis of the Nanoheterostructure. TiNT@AnNP was synthesized by a microwave-assisted alkaline hydrothermal method. For this, 3.00 g of anatase TiO_2 (Sigma-Aldrich, 99.8% purity, free from other metal ions, 60-80 nm average particle size) was dispersed in 90 mL of NaOH solution (10 mol L^{-1}) under magnetic stirring for 30 min and then transferred to a Teflon reactor, which was sealed and subjected to microwave irradiation (domestic micro-oven model Panasonic, 2.45 MHz, maximum power of 700 W) at 140°C for 3 h. The solid product obtained was washed with deionized water and vacuum dried for 24 h.

2.2. Characterization. XRD patterns were obtained with a Shimadzu XRD 6000 powder diffractometer with the use of Cu Kα radiation ($\lambda = 1.5406$ Å). Raman spectra were obtained with a Raman spectrometer (Senterra, Bruker) with a 2.33 eV laser excitation source. Scanning electron microscopy (SEM), energy-dispersive X-ray spectroscopy (EDS), and scanning transmission electron microscopy (STEM) were performed with a scanning electron microscope (FEI Quanta 250 FEG with an EDAX Genesis-Apollo X SDD detector attached). HRTEM and SAED were performed with an FEI Tecnai G^2 F20 instrument. N_2 adsorption–desorption analysis was conducted with a Belsorp mini II at 77 K up to 760 Torr. UV-visible diffuse reflectance spectroscopy of the samples was performed in absorbance mode with a Shimadzu UV-2600 spectrophotometer. For the optical bandwidth energy for an indirect transition, the Kubelka-Munk function was used [22]. The X-ray photoelectron spectra (XPS) were obtained with a Scienta Omicron ESCA+ spectrometer system equipped with an EA 125 hemispherical analyzer and an Xm 1000 monochromatic X-ray source (Al Kα, 1486.7 eV). The X-ray source was used with a power of 280 W as the spectrometer worked in a constant-pass energy

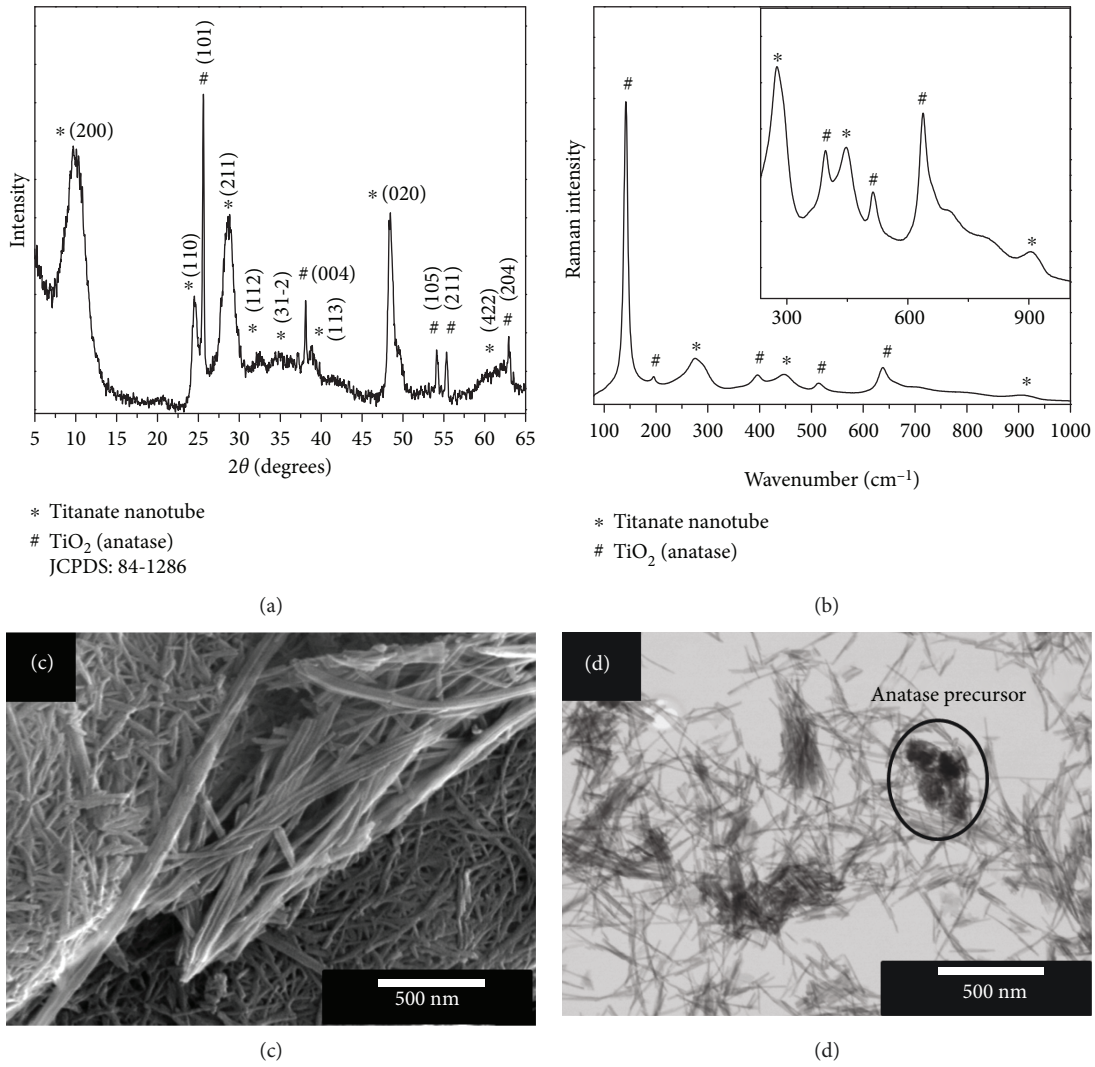

Figure 1: (a) X-ray diffraction and (b) Raman spectra of titanate nanotubes decorated with anatase nanoparticles (TiNT@AnNP); the inset shows the zoom in of the spectra in the 230-1000 cm^{-1} region to facilitate the visualization of the titanate-related bands. (c) Scanning electron micrograph and (d) scanning transmission electron micrograph of TiNT@AnNP; the existence of unreacted precursor anatase clusters is shown in the circle.

mode of 50 eV. A Scienta Omicron CN10 charge neutralizer with a beam energy of 1.6 eV charge was used to compensate the charge effect while the spectra were obtained. For corrections of peak shifts due to the remaining charge effect, the binding energies of all spectra were scaled with the use of the main peak of C 1*s* at 284.8 eV as a reference. Wide-scan spectra, for peak identification, were recorded with a step of 0.5 eV, and high-resolution spectra for core levels were obtained with the step of 0.03 eV. All the X-ray photoelectron spectra were analyzed with the software program CasaXPS, where the background in high-resolution spectra is computed by the Shirley method. Peak fitting of core levels was done with an asymmetric Gaussian-Lorentzian product function for the peak shape.

2.3. Photocatalytic Activity Test. In a typical photodegradation experiment with the anionic dye Remazol blue (RB), 350 mL of aqueous dye solution with a concentration of 50 mg L^{-1} was taken in a beaker and 200 mg of the catalyst added. The system was kept in a closed box and first stirred in the dark for 30 minutes with the aid of a magnetic stirrer to establish the adsorption-desorption equilibrium. It was observed that the absorbance bands of the RB dye did not decrease over time, which leads us to infer that the adsorption process does not occur or negligible. After the adsorption test, the actual photodegradation was carried out by immersing a mercury lamp (80 W, Philips, with emission at UV-visible range 380 nm-780 nm) inserted into a quartz tube. The solution was continued to be stirred under magnetic stirring, the temperature was maintained at 25 ± 5°C with a thermostatic bath, and excess oxygen was bubbled with an air pump. The rate of dye degradation was observed for 60 min, during which, aliquots were withdrawn at 0, 5, 10, 15, 20, 25, 30, 45, and 60 min,

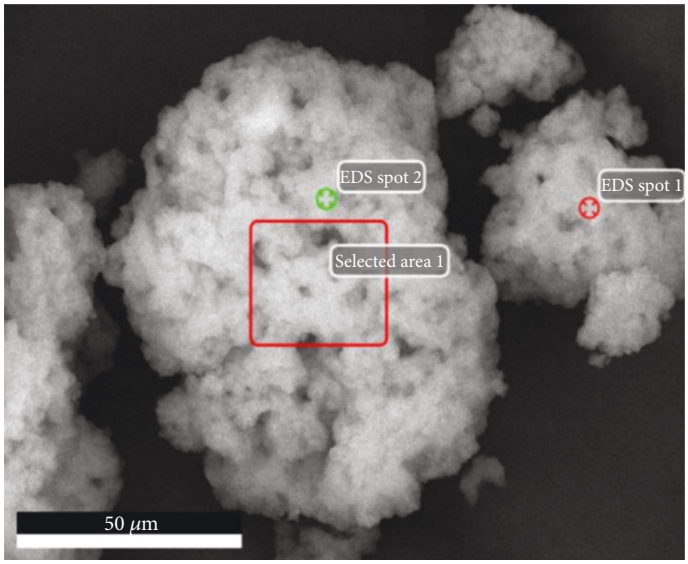

Elements (atomic %)	EDS spot 1	EDS spot 2	EDS area 1
O	66.34	65.53	61.41
Na	11.72	16.75	12.70
Ti	19.85	17.69	25.30

Figure 2: Elemental composition (Na, Ti, and O) of TiNT@AnNP probed by EDS in different parts of the sample, as shown in the attached SEM diagram.

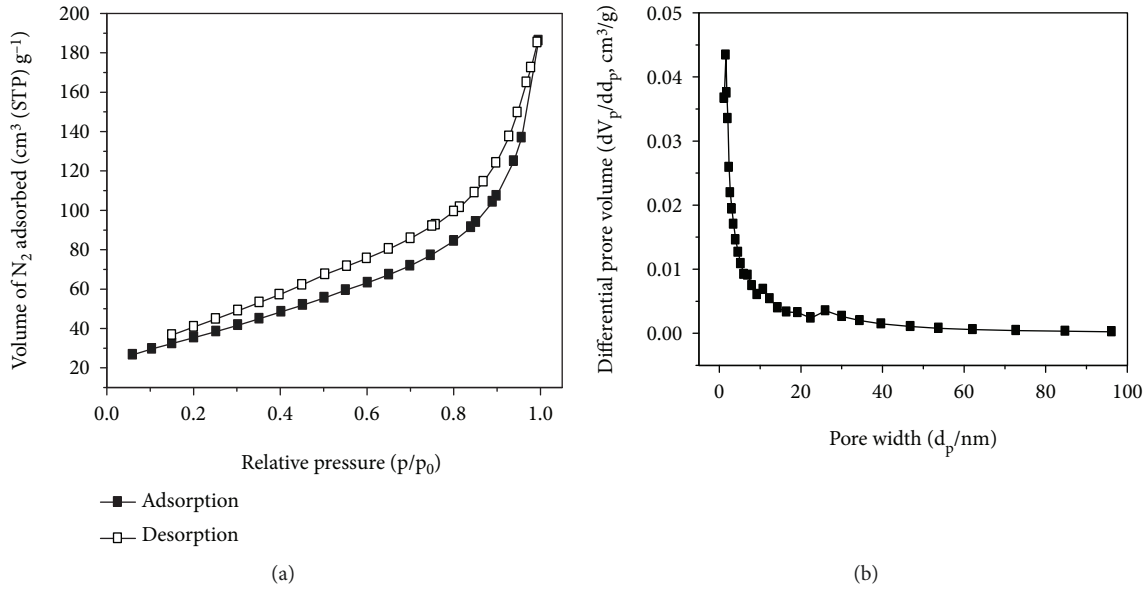

Figure 3: (a) N_2 adsorption-desorption isotherms and (b) pore size distribution of TiNT@AnNP.

centrifuged, and analyzed with a Shimadzu UV-3600 spectrophotometer (in absorbance mode). The dye concentration was determined by the corresponding value of the absorbance at $\lambda_{max} = 591$ nm. All photocatalysis experiments were performed in triplicate.

In order to study the influence of light on the degradation of the RB dye, in the absence of the catalyst, a photolysis study was carried out. The methodology was very similar to the typical photocatalysis experiment, described above, but without the catalyst. The results for photolysis (Supplementary Figure 1) indicated 49.5% degradation of the RB dye at the end of 60 minutes of irradiation in our reactor.

3. Results and Discussion

The XRD diffractograms (Figure 1(a)) show the characteristic diffraction peaks of the anatase phase of TiO_2 around $2\theta = 25^\circ$, 38°, 54°, 55°, and 63°, corresponding to the crystallographic planes (101), (004), (105), (211), and (204), respectively (JCPDS card no. 84-1286), and wider peaks characteristic of titanate nanotubes at $2\theta = 9.8^\circ$, 24°, 28°, and 48°, corresponding to the crystallographic planes (200), (110), (211), and (020), respectively, of titanate nanotubes [19, 23, 24]. After careful scrutiny, some other wider peaks with low intensities were assigned to the titanate nanotube structures centered around $2\theta = 32^\circ$, 34.8°, 38.8°, and 61.5°, corresponding to

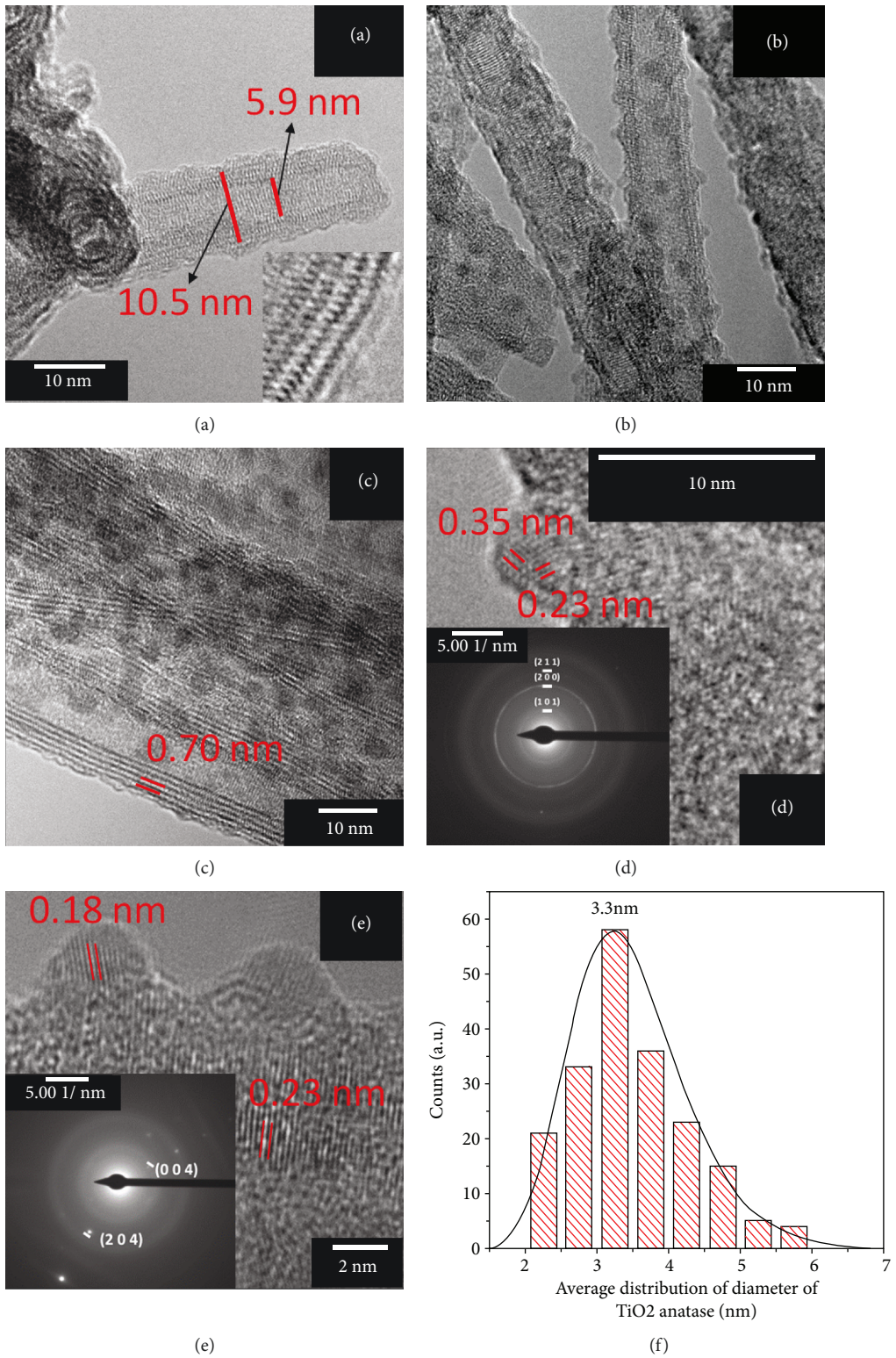

Figure 4: High-resolution transmission electron microscopy images of the titanate nanotubes decorated with anatase nanoparticles showing (a) the internal and external diameter of titanate nanotubes; the inset shows the TiO_6 octahedra, arranged in a zig-zag fashion, forming the walls of the titanate nanotubes. (b) Titanate nanotubes decorated with anatase nanocrystals, (c) interlamellar distance of the nanotubes, and (d, e) crystallite planes with corresponding d-spacings of the anatase nanoparticles decorating nanotubes; the insets in (d, e) show selected-area electron diffraction patterns showing a bright spot as well as concentric circles corresponding to these planes. (f) Diameter distribution of anatase nanoparticles, showing an average particle diameter of 3.3 nm.

the crystallographic planes (112), (31-2), (113), and (422), respectively, characteristic of titanate nanotubes [25].

The interlamellar distance of the nanotubes (d_{200}) was calculated with Bragg's law and was 0.87 nm, which matches with a structure similar to sodium trititanate, $Na_2Ti_3O_7$, according to previous literature [26, 27]. The interplanar distances of the planes of the anatase phase were also calculated with Bragg's law and were $d_{101} = 0.35$ nm, $d_{004} = 0.24$ nm, $d_{200} = 0.18$ nm, $d_{105} = 0.17$ nm, $d_{211} = 0.16$ nm, and $d_{204} = 0.15$ nm. The mean crystallite size of the anatase particle was calculated to be approximately 65 nm from the sharpest anatase peak at $2\theta \approx 25^\circ$, which corresponds to the unreacted precursor, also identified in the STEM image (Figure 1(d)). The Raman spectrum (Figure 1(b)) shows vibrational modes corresponding to the anatase phase at 142, 196, 395, 515, and 638 cm^{-1}, as well as vibrational modes of titanate nanotubes at 280, 448, and 908 cm^{-1}, emphasized in the inset of Figure 1(b) [28, 29]. It was possible to confirm the formation of titanate nanotubes starting from the anatase precursor with the structural information obtained from the XRD patterns and Raman spectra and the morphological data obtained by scanning electron microscopy and STEM (Figures 1(c) and 1(d)).

The chemical composition of the titanate nanotubes was investigated by energy-dispersive X-ray spectroscopy (EDS). The atomic percentages of the elements were shown in Figure 2, which leads to the Na/Ti and Ti/O atomic ratios to be 0.66 and 0.32, respectively. These values suggest a $Na_2Ti_3O_7$ phase structure [30] with a small excess of oxygen, probably due to the presence of water in the structure.

The N_2 adsorption-desorption isotherms at 77 K of TiNT@AnNP were shown in Figure 3(a), which shows a mixed II-type IV nature with a small H4 hysteresis loop, characteristic to the titanate nanotubes, reflective of its mesoporous nature [31]. The specific surface area was calculated using the Brunauer-Emmet-Teller (BET) method which showed a drastic increase of the BET surface area of TiNT@AnNP (127 m^2/g) compared to that of the anatase-TiO_2 precursor material (15 m^2/g). The pore size distribution of TiNT@AnNP was shown in Figure 3(b), and the average pore diameter as well as the total pore volume was calculated using Brunauer-Joyner-Halenda (BJH) method and was found to be 8.7 nm and 0.26 cm^3/g, respectively, confirming the mesoporous nature.

To carefully study TiNT@AnNP, HRTEM was performed rigorously, and surprisingly the titanate nanotubes were found to be homogeneously and intensively decorated with anatase nanoparticles. Representative HRTEM images are shown in Figures 4(a)–4(e). The internal and external diameters of the titanate nanotubes were 5.9 and 10.5 nm, respectively (Figure 4(a)). A close zoom in of the wall structure of the titanate nanotube shows the TiO_6 octahedra, connected in zig-zag fashion, depicted in the inset of the Figure 1. However, a previously unreported feature was observed: titanate nanotubes appear to be uniformly decorated with anatase nanocrystals after the microwave hydrothermal reaction (Figure 4(b)), giving rise to a nanoheterostructure. The interlamellar spacing between the multilayers of the

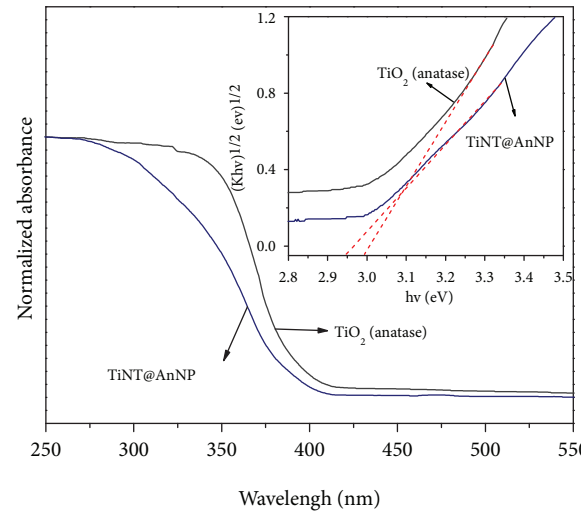

FIGURE 5: UV-visible diffuse reflectance spectra of TiO_2 (anatase) and titanate nanotubes decorated with anatase nanoparticles (TiNT@AnNP) and band gap obtained by the Kubelka-Munk method (inset).

nanotubes measured by HRTEM was 0.70 nm (Figure 4(c)). The reduction of the interlayer distance (compared with the value obtained by XRD) could be rationalized by the fact that for HRTEM analysis, the sample was subjected to a high vacuum, which resulted in the release of water from the titanate layers, promoting a shortening of the distance between the layers [32].

The SAED patterns of TiNT@AnNP shown in the insets in Figures 4(d) and 4(e) indicate the predominance of diffuse concentric rings [25], but because of the low crystallinity of the titanate tubes, it was difficult to assign the planes of this phase. However, concentric rings associated with the more crystalline phase related to anatase nanocrystals were seen in the SAED images, corresponding to the different Bragg planes, especially (101), (004), (200), (211), and (204). The interplanar distances of the anatase nanocrystals of the heterostructure were measured from the HRTEM images (Figures 4(d) and 4(e)) directly and were found to be $d_{101} = 0.35$ nm, $d_{004} = 0.23$ nm, and $d_{200} = 0.18$ nm, which corroborates the values found by XRD as well as SAED. If carefully observed, an amorphous interface can be seen between these two crystalline phases, titanate nanotubes and anatase nanoparticles, which can be clearly seen in Figure 4(e). This is a site with structural defects, which could be responsible for the electron trapping, stopping the electron-hole pair recombination and therefore leading to better photooxidation of the dyes. The average diameter distribution of the anatase nanoparticles of TiNT@AnNP is shown in Figure 4(f) and was 3.3 nm.

The UV-visible (solid) absorption spectra of TiNT@AnNP and the anatase precursor are shown in Figure 5. The band gaps of the corresponding spectra were evaluated by the Kubelka-Munk method [22] and are shown in the inset in Figure 5. The results indicate that the formation of TiNT@AnNP resulted in a change in the electronic levels of

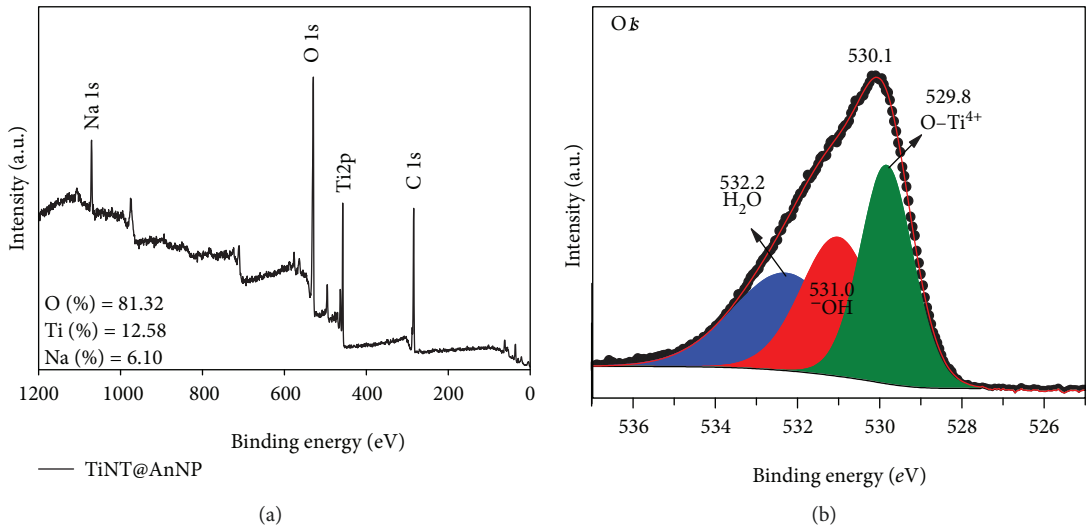

Figure 6: (a) Full scan X-ray photoelectron spectroscopy of TiNT@AnNP; (b) O 1s spectra deconvoluted into subpeaks.

the anatase precursor as the band gap decreased to 2.94 eV (nanoheterostructure) from 2.99 eV (anatase). Although the change is small, the enhanced photocatalytic activity of TiNT@AnNP in the degradation of Remazol blue can be attributed to the synergism associated with the mixed phase and defect-rich phase boundaries, which increases the efficiency of generating electron-hole pairs.

The XPS (Figure 6(a), the maximum energy for C 1*s* (284.8 eV) was used as the reference binding energy) reveals the surface compositional information of the TiNT@AnNP. The surface elemental composition of the TiNT@AnNP was found to be $Na_2Ti_{4.12}O_{26.68}$ (Figure 6(a)), with a higher compositional value of both Ti and O compared to that found from EDS, mentioned earlier. This may be attributed to the surface sensitivity of the XPS method, as it takes up the additional signals of Ti and O from the anatase-TiO_2 nanoparticles, decorated on the surface of the tubes. Further excess of O can be accounted for the structural water as O 1*s* spectrum of TiNT@AnNP (Figure 6(b)) shows that the O 1*s* peak at 530.1 eV can be deconvoluted into subpeaks at 532, 531, and 529.8 eV, which are attributed to H_2O, –OH, and Ti–O, respectively. Similar results were reported by Kim et al. [33], who found that the O 1*s* peak is formed from Ti–O in TiO_2 and OH in Ti–OH. The higher intensity of the Ti–OH groups in TiNT@AnNP indicates the presence of a large amount of surface hydroxyl groups [6].

Although the stepwise formation of TiNT@AnNP from anatase particles was investigated thoroughly in this work, two possible mechanisms are suggested from a study of the literature and indirect evidence and are shown in the schemes in Figure 7. Because trititanate nanotubes have building blocks similar to those of anatase TiO_2, the former can be converted to the latter by simple chemical routes. In acidic conditions, this transformation follows a topochemical reaction mechanism, whereas in alkaline conditions it proceeds through a dissolution and nucleation mechanism [34]. There has been much controversy about the exact mechanism of the formation of titanate nanotubes from anatase TiO_2 via an alkaline hydrothermal synthesis route, but there is agreement in that to begin with the surface of the starting material, anatase particles, which is delaminated in an alkaline medium, giving rise to smaller entities such as $Ti(OH)_4$, and then recrystallizes to form trititanate nanosheets, which roll up to form nanotubes [35]. In our first proposed mechanism (path 1 in Figure 7), it is surmised that because of the superefficient, rapid, and less selective internal heating by microwaves, all the aforementioned processes probably happen simultaneously and at an elevated rate in the reactor. As the precursor anatase particles is dissolved in NaOH, generating $Ti(OH)_4$, they crystallize not only as trititanate sheets, which then roll up to form titanate nanotubes, but also as anatase nanocrystals of smaller diameter (3-4 nm), which can precipitate on the surface of the nanotube, formed at the same time, and are attached with the help of dangling hydroxyl groups on the titanate nanotube surface, thereby generating the observed TiNT@AnNP heterostructure. As an alternative, we propose another two-step mechanism, depicted in Figure 7 as path 2, where the titanate nanotube is first generated by the dissolution-recrystallization pathway from the anatase particles, followed in the second step by corrosion of the wall of the tubes in alkaline solution to generate $Ti(OH)_4$, which recrystallizes as anatase nanocrystals over the nanotubes. A similar mechanism was observed in conventional alkaline hydrothermal posttreatment of sodium trititanate nanotubes, where the surface of the sodium trititanate tube slowly decomposes to produce $Ti(OH)_4$ fragments, which rearrange themselves through dehydration, giving rise to a Ti–O–Ti linkage, eventually seeding to form a tetragonal faceted single crystal of anatase TiO_2 [9]. Because of the fast kinetics and the stochastic nature of the reaction happening in the microwave reactor, it is impossible at this stage to choose between these two pathways, but careful observation of the HRTEM images of the reaction conducted for 1 and 4 h in conditions similar to those described above shows that the nanocrystals obtained in the latter case are larger than those obtained in the former case (shown in Supplementary

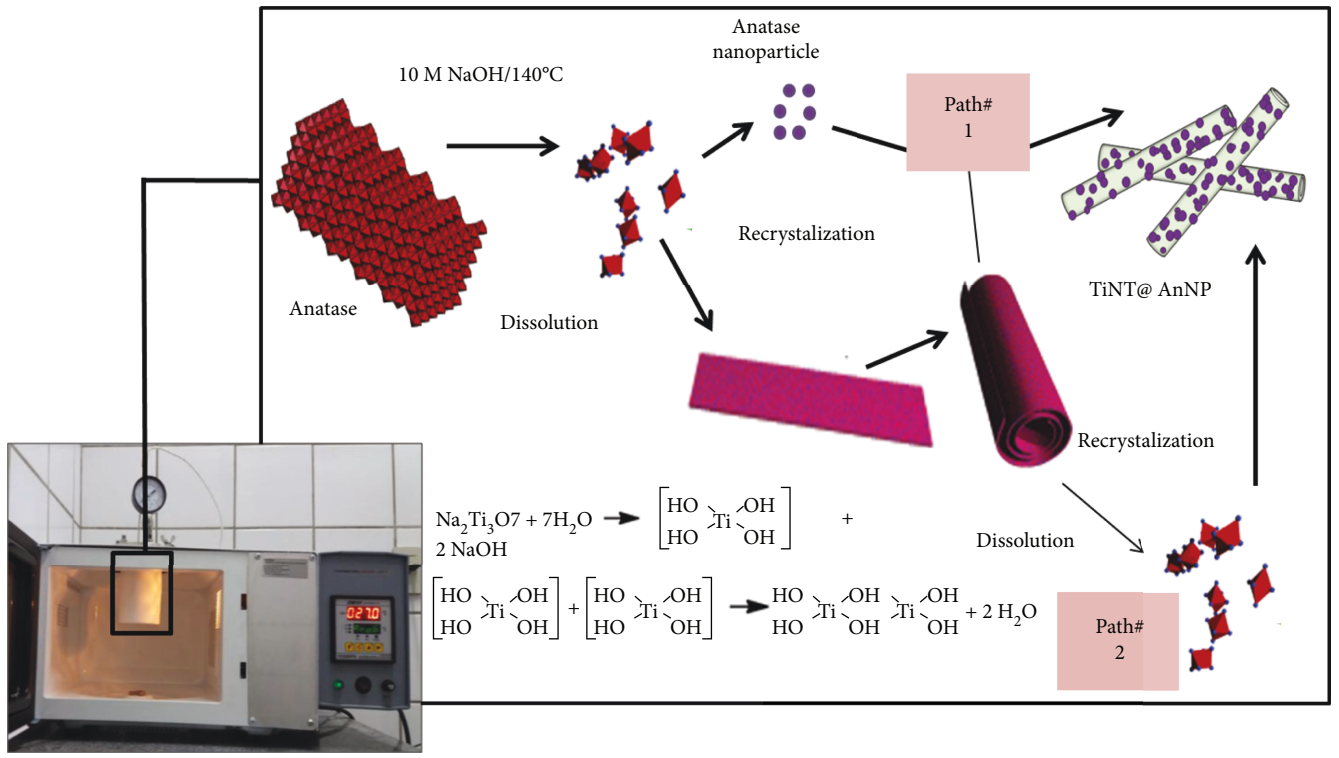

Figure 7: Two possible mechanisms for the formation of titanate nanotubes decorated with anatase nanoparticles (TiNT@AnNP) by microwave-assisted hydrothermal synthesis (the figure was created based on the observation of reference [33]).

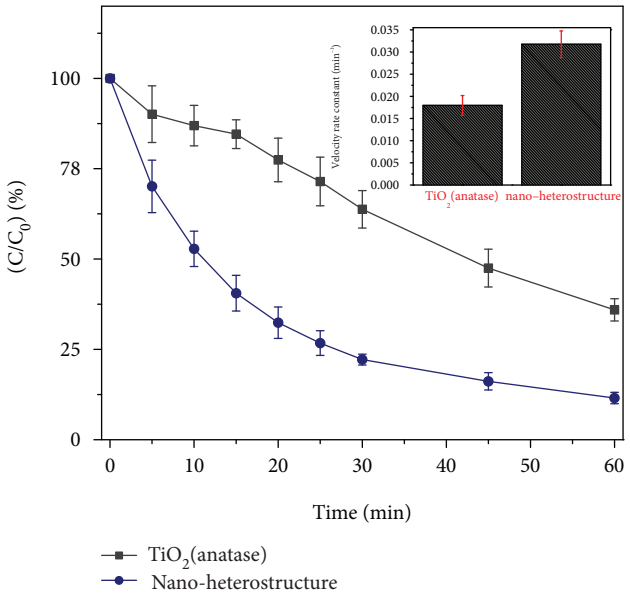

Figure 8: Photocatalytic degradation of Remazol blue as a function of the irradiation time under visible light for the anatase precursor and the titanate nanotubes decorated with the anatase nanoparticles obtained, triplicated; the inset shows the rate constants of the degradation experiment, triplicated, considering the Langmuir-Hinshelwood pseudo-first-order kinetic pathway.

Figure 2), which suggests that the second possibility (path 2 in Figure 7) is more likely, which is promoting the ripening of anatase nanoparticles.

Experiments investigating the photocatalytic degradation of the anionic dye Remazol blue by TiNT@AnNP as well as the precursor were performed under UV-visible light irradiation (Figure 8). At the beginning of the photocatalysis experiment, the photocatalysts were added to the solution (50 mg/L) of the dye Remazol blue and agitated for 30 minutes in the dark. Then the concentration of the solution was measured by means of UV-Vis spectroscopy, and it was found unchanged, i.e., no significant adsorption of the dye was observed by the catalyst under the experimental conditions. In both cases, degradation followed the Langmuir-Hinshelwood pseudo-first-order kinetics model, as shown by the best fit with a correlation coefficient $(R^2) = 0.953$ and 0.977, respectively. The degradation rate constant was 0.0317 min^{-1} for TiNT@AnNP, whereas for the anatase precursor, it was 0.017 min^{-1}. The rate constant and the degradation capacity, as shown in Figure 8, for the hybrid system compared with the precursor material were much greater, indicating that a microwave-assisted hydrothermal synthesis is an alternative option for fast and efficient one-pot production of a catalyst, which can be used for complete degradation of the dye Remazol blue.

4. Conclusion

A nanoheterostructure of a titanate nanotube decorated with anatase nanoparticles was generated by a one-pot microwave-assisted hydrothermal method with anatase as the precursor; this had not been reported previously.

Morphological and structural characterization showed that these anatase nanoparticles are anchored on the titanate nanotubes with a homogeneous distribution and have an average diameter of 3.3 nm. Two possible mechanisms for the formation of the heterostructure were proposed, and the mechanism involving the formation of titanate nanotubes followed by corrosion of the walls by NaOH and recrystallization of anatase nanocrystals over the nanotube surface was argued to be more likely because the longer synthesis produces larger anatase nanoparticles on nanotubes. Finally, TiNT@AnNP was investigated for its ability to degrade the anionic dye Remazol blue photocatalytically, and it was found to be more efficient than the precursor TiO_2 (anatase), probably because of its greater surface area and efficiency of separation of photoinduced electron-hole pairs. Thus, the microwave-assisted hydrothermal route can be used as an alternative efficient and one-pot method to generate TiNT@AnNP with increased efficiency for photodegradation of dyes.

Data Availability

The data used to support the findings of this study are available from the corresponding author upon request.

Conflicts of Interest

The authors declare no conflict of interest.

Authors' Contributions

The manuscript was written through the contribution of all authors, specifically: conceptualization, B.C.V., A.O.L., A.G., J.A.O.O., R.R.M.S, C.L., and O.P.F.; methodology, S.B.S.G., A.G., J.A.O.O., T.M.F.M., and B.C.V.; investigation, S.B.S.G., A.G., A.O.L., J.A.O.O., T.M.F.M, O.P.F., and B.C.V.; resources, B.C.V.; supervision, B.C.V. and A.G.; project administration, B.C.V.; funding acquisition, B.C.V., O.P.F, and A.O.L. All authors have given their approval to the final version of the manuscript.

Acknowledgments

The authors gratefully acknowledge the financial support from the Brazilian funding agencies FAPEPI (grant 001/2018), CAPES (Procad 2013 grant 183995), and CNPq (grants 305632/2016-7 and PVE 400397/2014-5). A.O.L. would like to thank CNPq (grant 303752/2017-3) for the financial support.

Supplementary Materials

The Supplementary Material contains information about the photolysis experiment of the Remazol blue (RB) dye solution using HG lamp for 60 min (without the photocatalyst), showing the low degradation of RB without the photocatalyst. Also, it presents HRTEM images of the titanate nanotubes decorated with anatase nanoparticles synthesized at 1 h and 4 h, showing larger anatase nanoparticles in the sample treated at 4 h than 1 h. *(Supplementary Materials)*

References

[1] Y. Zhang, Z. Jiang, J. Huang et al., "Titanate and titania nanostructured materials for environmental and energy applications: a review," *RSC Advances*, vol. 5, no. 97, pp. 79479–79510, 2015.

[2] Y. L. Pang, S. Lim, H. C. Ong, and W. T. Chong, "A critical review on the recent progress of synthesizing techniques and fabrication of TiO2-based nanotubes photocatalysts," *Applied Catalysis A: General*, vol. 481, pp. 127–142, 2014.

[3] H.-H. Ou and S.-L. Lo, "Review of titania nanotubes synthesized via the hydrothermal treatment: fabrication, modification, and application," *Separation and Purification Technology*, vol. 58, no. 1, pp. 179–191, 2007.

[4] D. S. Xu, J. M. Li, Y. X. Yu, and J. J. Li, "From titanates to TiO_2 nanostructures: controllable synthesis, growth mechanism, and applications," *Science China Chemistry*, vol. 55, no. 11, pp. 2334–2345, 2012.

[5] R. Doong and C. Tsai, "Synergistic effect of Cu adsorption on the enhanced photocatalytic degradation of bisphenol A by TiO_2/titanate nanotubes composites," *Journal of the Taiwan Institute of Chemical Engineers*, vol. 57, pp. 69–76, 2015.

[6] F. Chen, Y. Li, Z. Liu, and P. Fang, "Facile synthesis of TiO_2/-trititanate heterostructure with enhanced photoelectric efficiency for an improved photocatalysis," *Applied Surface Science*, vol. 341, pp. 55–60, 2015.

[7] F. Alvarez-Ramirez and Y. Ruiz-Morales, "Ab initio molecular dynamics calculations of the phase transformation mechanism for the formation of TiO_2 titanate-type nanosheets from anatase," *Chemistry of Materials*, vol. 19, no. 12, pp. 2947–2959, 2007.

[8] H. Y. Zhu, Y. Lan, X. P. Gao et al., "Phase transition between nanostructures of titanate and titanium dioxides via simple wet-chemical reactions," *Journal of the American Chemical Society*, vol. 127, no. 18, pp. 6730–6736, 2005.

[9] J. Li and D. Xu, "Tetragonal faceted-nanorods of anatase TiO_2 single crystals with a large percentage of active {100} facets," *Chemical Communications*, vol. 46, no. 13, pp. 2301–2303, 2010.

[10] L. Zhang, H. Lin, N. Wang, C. Lin, and J. Li, "The evolution of morphology and crystal form of titanate nanotubes under calcination and its mechanism," *Journal of Alloys and Compounds*, vol. 431, no. 1-2, pp. 230–235, 2007.

[11] A. Sandoval, R. Zanella, and T. E. Klimova, "Titania nanotubes decorated with anatase nanocrystals as support for active and stable gold catalysts for CO oxidation," *Catalysis Today*, vol. 282, pp. 140–150, 2017.

[12] H. Zhu, X. Gao, Y. Lan, D. Song, Y. Xi, and J. Zhao, "Hydrogen titanate nanofibers covered with anatase nanocrystals: a delicate structure achieved by the wet chemistry reaction of the titanate nanofibers," *Journal of the American Chemical Society*, vol. 126, no. 27, pp. 8380-8381, 2004.

[13] H. Yu, J. Yu, B. Cheng, and M. Zhou, "Effects of hydrothermal post-treatment on microstructures and morphology of titanate nanoribbons," *Journal of Solid State Chemistry*, vol. 179, no. 2, pp. 349–354, 2006.

[14] D. M. P. Mingos and D. R. Baghurst, "Tilden lecture. Applications of microwave dielectric heating effects to synthetic problems in chemistry," *Chemical Society Reviews*, vol. 20, pp. 1–47, 1991.

[15] T. Kasuga, M. Hiramatsu, A. Hoson, T. Sekino, and K. Niihara, "Formation of titanium oxide nanotube," *Langmuir*, vol. 14, no. 12, pp. 3160–3163, 1998.

[16] Y.-a. Wang, J. Yang, J. Zhang, H. Liu, and Z. Zhang, "Microwave-assisted preparation of titanate nanotubes," *Chemistry Letters*, vol. 34, no. 8, pp. 1168-1169, 2005.

[17] S. H. Cho, N. H. Hao, and T. Yamaguchi, "Comparative analysis and characterization of TiO2 nanotubes produced by microwave assisted hydrothermal method and normal hydrothermal," *Journal of Ceramic Processing Research*, vol. 17, no. 1, pp. 41–45, 2016.

[18] M. C. Manique, A. P. Silva, A. K. Alves, and C. P. Bergmann, "Titanate nanotubes produced from microwave-assisted hydrothermal synthesis: characterization, adsorption and photocatalytic activity," *Brazilian Journal of Chemical Engineering*, vol. 34, no. 1, pp. 331–339, 2017.

[19] D. C. Manfroi, A. dos Anjos, A. A. Cavalheiro, L. A. Perazolli, J. A. Varela, and M. A. Zaghete, "Titanate nanotubes produced from microwave-assisted hydrothermal synthesis: photocatalytic and structural properties," *Ceramics International*, vol. 40, no. 9, Part A, pp. 14483–14491, 2014.

[20] S. Preda, M. Rutar, P. Umek, and M. Zaharescu, "A study of thermal properties of sodium titanate nanotubes synthesized by microwave-assisted hydrothermal method," *Materials Research Bulletin*, vol. 71, pp. 98–105, 2015.

[21] S. Ribbens, V. Meynen, G. V. Tendeloo et al., "Development of photocatalytic efficient Ti-based nanotubes and nanoribbons by conventional and microwave assisted synthesis strategies," *Microporous and Mesoporous Materials*, vol. 114, no. 1-3, pp. 401–409, 2008.

[22] S. Valencia, J. M. Marın, and G. Restrepo, "Study of the bandgap of synthesized titanium dioxide nanoparticules using the sol-gel method and a hydrothermal treatment," *The Open Materials Science Journal*, vol. 4, no. 1, pp. 9–14, 2010.

[23] B. C. Viana, O. P. Ferreira, A. G. Souza Filho, A. A. Hidalgo, J. Mendes Filho, and O. L. Alves, "Highlighting the mechanisms of the titanate nanotubes to titanate nanoribbons transformation," *Journal of Nanoparticle Research*, vol. 13, no. 8, pp. 3259–3265, 2011.

[24] C.-K. Lee, C.-C. Wang, M.-D. Lyu, L.-C. Juang, S.-S. Liu, and S.-H. Hung, "Effects of sodium content and calcination temperature on the morphology, structure and photocatalytic activity of nanotubular titanates," *Journal of Colloid and Interface Science*, vol. 316, no. 2, pp. 562–569, 2007.

[25] Q. Chen, G. H. Du, S. Zhang, and L.-M. Peng, "The structure of trititanate nanotubes," *Acta Crystallographica Section B Structural Science*, vol. 58, no. 4, pp. 587–593, 2002.

[26] E. Morgado, M. A. S. de Abreu, G. T. Moure, B. A. Marinkovic, P. M. Jardim, and A. S. Araujo, "Characterization of nanostructured titanates obtained by alkali treatment of TiO_2-anatases with distinct crystal sizes," *Chemistry of Materials*, vol. 19, no. 4, pp. 665–676, 2007.

[27] V. C. Ferreira and O. C. Monteiro, "New hybrid titanate elongated nanostructures through organic dye molecules sensitization," *Journal of Nanoparticle Research*, vol. 15, 2013.

[28] B. C. Viana, O. P. Ferreira, A. G. S. Filho, A. A. Hidalgo, J. M. Filho, and O. L. Alves, "Alkali metal intercalated titanate nanotubes: a vibrational spectroscopy study," *Vibrational Spectroscopy*, vol. 55, no. 2, pp. 183–187, 2011.

[29] M. A. Cortés-Jácome, G. Ferrat-Torres, L. F. F. Ortiz et al., "In situ thermo-Raman study of titanium oxide nanotubes," *Catalysis Today*, vol. 126, no. 1-2, pp. 248–255, 2007.

[30] O. P. Ferreira, A. G. Souza Filho, J. Mendes Filho, and O. L. Alves, "Unveiling the structure and composition of titanium oxide nanotubes through ion exchange chemical reactions and thermal decomposition processes," *Journal of the Brazilian Chemical Society*, vol. 17, no. 2, pp. 393–402, 2006.

[31] M. Thommes, K. Kaneko, A. V. Neimark et al., "Physisorption of gases, with special reference to the evaluation of surface area and pore size distribution (IUPAC Technical Report)," *Pure and Applied Chemistry*, vol. 87, no. 9-10, 2015.

[32] T. M. F. Marques, C. Luz-Lima, M. Sacilloti et al., "Photoluminescence enhancement of titanate nanotubes by insertion of rare earth ions in their interlayer spaces," *Journal of Nanomaterials*, vol. 2017, Article ID 3809807, 9 pages, 2017.

[33] G. S. Kim, S. G. Ansari, H. K. Seo, Y. S. Kim, and H. S. Shin, "Effect of annealing temperature on structural and bonded states of titanate nanotube films," *Journal of Applied Physics*, vol. 101, no. 2, article 024314, 2007.

[34] J. Li, H. Yang, Q. Li, and D. Xu, "Enlarging the application of potassium titanate nanowires as titanium source for preparation of TiO_2 nanostructures with tunable phases," *CrystEngComm*, vol. 14, no. 9, 2012.

[35] Á. Kukovecz, M. Hodos, E. Horváth, G. Radnóczi, Z. Kónya, and I. Kiricsi, "Oriented crystal growth model explains the formation of titania nanotubes," *The Journal of Physical Chemistry B*, vol. 109, no. 38, pp. 17781–17783, 2005.